# J3.5 OUTDOOR SCALE MODEL EXPERIMENT TO EVALUATE THE COMPLETE URBAN SURFACE TEMPERATURE

Sarah M. Roberts[1,*], J.A. Voogt[2], and T. R. Oke[1]
[1] University of British Columbia, Vancouver, B.C., Canada; [2] University of Western Ontario, London, ON, Canada

## 1. INTRODUCTION

Much of our current understanding of the physical processes that contribute to urban climate is derived from field studies conducted in real cities using a range of ground-based and airborne measurement techniques. Insight is also gained from wind tunnel modeling because it allows isolation and simplification of climatic processes through control of the impinging flow and the properties of surface structures (Plate, 1999). Data from both approaches are used to construct, evaluate, and validate numerical models which further aid our understanding of urban climate processes. However, the inherent complexity of surface morphology and energetic exchanges of real-world urban environments still poses challenges to numerical modeling of urban environments. Outdoor physical scale modeling is a potentially powerful compromise between wind tunnel modeling and full-scale observation because it incorporates the experimental control of physical and numerical modeling but preserves some of the real complexities associated with natural environmental forcing (e.g. atmospheric turbulence and radiation loading; Mills, 1997).

Here we describe the project design and preliminary results of an open-air physical scale model experiment to investigate three-dimensional (i.e., complete) facet surface temperatures within an idealized urban array. In addition to providing a detailed analysis of the variation in observed facet temperatures, the resulting dataset can be used to evaluate radiation emissions and a model to optimize sensor placement.

## 2. SCALE MODEL SIMILARITY

Given that reduced-scale physical models are unable to fully replicate the complex morphology of cities and their meteorological exchange processes, it is difficult for these models to satisfy all of the similarity requirements considered important in scale modeling. Geometrical similarity, which is the primary modeling objective of the present experiment, is entirely feasible so long as the collection of roughness elements is scaled to generally match the relative size, dimension, and spatial distribution of real-world urban surface elements (Kanda, 2006). To achieve similarity in reduced-scale modeling of radiation emissions from a densely built-up urban setting it is necessary to ensure the physical processes governing these exchanges are suitably scaled. The characteristic length scale of radiation ($10^{-7}$ – $10^{-4}$ m) is considered negligible compared to the linear scale of even a small scale model (Oke, 1981). Hence placing the model outdoors, where it is subjected to the downward components of short- and longwave radiation, ensures similarity of radiation always exists. Matching of surface albedo, surface emissivity, and thermal mass is not rigorously undertaken here, however, actual building materials are used to construct the model.

## 3. METHODS

### 3.1 *Site*

The array was constructed on a rooftop at Arizona State University (ASU) in Tempe, Arizona and observations were conducted from November 2006 – January 2007, a period characterized by clear skies, modest precipitation and low atmospheric humidity. These conditions provide a robust regime of daytime heating-nighttime cooling of surfaces representative of those observed at many full-scale arid urban sites. The model assembly consisted of 40 cm x 40 cm x 25 cm scaled “buildings” constructed of hollow concrete masonry blocks with solid capping slabs (Figure 1) situated on a surface constructed of 1.2 m x 1.3 cm x 2.4 m polystyrene sheets overlain with 1.2 m x 1.3 cm x 2.4 m fiberboard sheets. Experimental configurations of the 13 x 13 m array included: three different canyon aspect ratios (H/W = 1.25,

*Corresponding author address:* Sarah Roberts, Dept. of Geography, University of British Columbia, 1984 West Mall, Vancouver, B.C. Canada V6T 1Z2; e-mail: sroberts@geog.ubc.ca

0.63, and 0.42), three different 'roof' albedo values and different 'roof' angles and orientations. Results reported here focus on variations arising from differences in canyon aspect ratio.

**Figure 1** Outdoor scale model constructed on a rooftop in Tempe, Arizona.

### 3.2 *Measurements*

Surface temperature measurements were conducted using twelve 28° half angle FOV infrared thermocouples (Apogee Instruments Inc., Model IRTS-P) located in the northeast corner of the model array. These sensors are sensitive in the 6.5 to 14 $\mu$m waveband and are capable of measuring surface temperatures between -10°C to +55°C to a precision of 0.3°C. The sensors were positioned to sample east-, west-, south-, and north-facing walls (two sensors per wall), one flat roof, one north-south oriented street, one east-west oriented street, and one street intersection (Figure 2). Thermal images to supplement the surface temperature measurements from the IRTc

**Figure 2** Installation of the Apogee IRTS-P infrared thermometers (IRTc) to measure surface temperatures of horizontal (roof, roads, and street intersection) surfaces (left) and walls (right).

array were captured by a FLIR Thermacam™, Model S-60 infrared camera positioned at various locations around the array perimeter throughout the experimental period. IDRISI© image processing software was used to extract individual facet surface temperatures from each image. A Kipp & Zonen CNR1 net radiometer located at the center of the array domain at a height of 161 cm above the ground continuously and independently monitored all four components of the surface radiation budget. Source area calculations show approximately 93% of the upwelling radiative flux signals sensed by the down-facing radiometers originated from the array surface.

### 3.3 *The complete urban surface*

Specification of the urban surface is crucial from a climatological perspective, for it is at the surface where sources and sinks of heat, mass, and momentum are located (Voogt and Oke, 1997). Depending on the scale of the processes under study and the position of observation several definitions of the urban surface are commonly used. For example: a plane at the ground that does not include roofs; a bird's-eye view that does not include vertical surfaces, or a plane at roof level that treats the canopy as a 'black box'. Ideally, the complete urban surface area comprises the boundary between the air and every element comprising the surface system.

The complete active surface area $A_C$ of each array configuration is estimated by adding the three-dimensional areas of walls, roofs, streets, and street intersections as given in Table 1. Individual facet surface temperatures are combined in proportion to their area fraction in order to estimate the complete surface temperature $T_C$ of a building unit. A Sensor-Surface-Sun Urban Model (SUM; Soux *et al.*, 2004) is used to calculate the view factors of surface components (walls, roofs, and streets) contained within the field-of-view (FOV) of a radiometer that measured a hemispherical radiative temperature, $T_{rad}$.

## 4. RESULTS

For each array configuration, one 24-hour period characterized by cloudless skies is selected for analysis. Using observed facet temperatures, the surface temperature is estimated for a building unit. The temperatures also provide the means to compare with three other conceptualizations of the urban surface (ground-level, roof-top, and bird's-eye view).

### 4.1 *Observed facet temperatures*

An example of the diurnal pattern of observed temperature of all facets comprising the complete urban surface is shown in Figure 3. Air

**Table 1** Surface component areas for each array configuration. All areas have units of $cm^2 \times 10^2$

| Area | **H/W = 1.25** | % of $A_c$ | **H/W = 0.63** | % of $A_c$ | **H/W = 0.42** | % of $A_c$ |
|---|---|---|---|---|---|---|
| Plan (2D) | 36 | 47 | 64 | 62 | 100 | 71 |
| Street (N-S or E-W) | 16 | 21 | 32 | 31 | 48 | 34 |
| Street intersection | 4 | 5 | 16 | 15 | 36 | 26 |
| Roof | 16 | 21 | 16 | 15 | 16 | 11 |
| Wall (N, S, E, or W) | 40 | 53 | 40 | 39 | 40 | 29 |
| Complete | 76 | | 104 | | 140 | |
| Total Active (3D/2D) | 2.1 | | 1.6 | | 1.4 | |

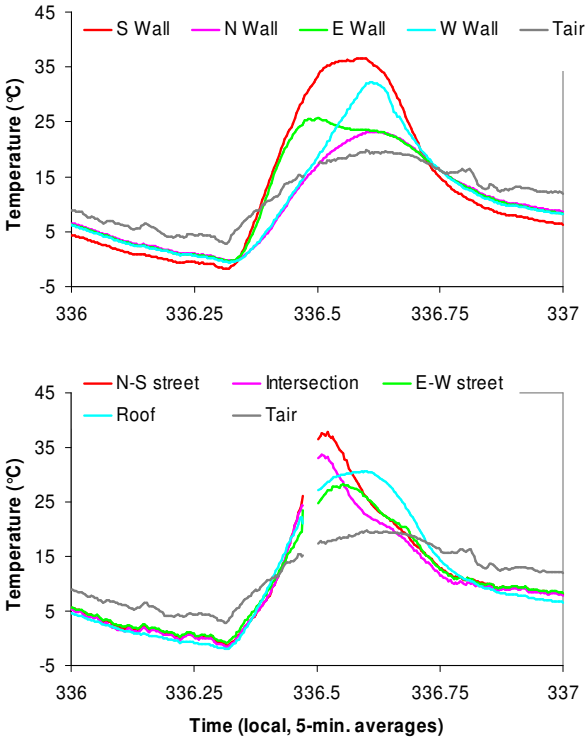


**Figure 3** Diurnal variation of individual vertical surfaces (top) and horizontal surfaces (bottom) for H/W = 1.25.

temperature at 1 m is also included. The thermal behavior of each facet follows a predictable pattern corresponding to the timing and duration of solar exposure. South-facing walls achieve the greatest daytime temperature, with north-facing walls being the coolest of the four vertical facets. East-facing walls peak earliest in the day at around noon, approximately three hours before the west-facing walls reach their maximum daily temperature. North-south streets and intersections follow a similar warming and cooling pattern, quickly achieving their peak values at around noon, when fully exposed to the sun. East-west streets remain largely shaded at this time of year and thus do not demonstrate as large a diurnal temperature range as other horizontal surfaces.

Contrary to the thermal behavior commonly observed in most real-world urban settings even under full solar exposure, roof surfaces remain cooler than street surfaces. The 2.5 cm solid concrete capping slabs simulating roof surfaces have much larger thermal mass than the same thickness of the combined polystyrene-fiberboard sheeting simulating the ground surfaces. The ground surfaces, therefore, have a more robust thermal response to solar heating, causing a relatively sharp rise and fall of their surface temperatures near midday.

### 4.2 *Comparison of complete urban surface definitions*

Figure 4 shows the difference in surface temperature between $T_C$ and that of bird's-eye view, ground-level, and roof-top definitions of the urban surface for each array configuration. A comparison between $T_C$ and the hemispherical radiative temperature $T_{rad}$ is also plotted.

Some common patterns are seen between the three array configurations. The least amount of bias between $T_C$ and other temperature measures occurs at night, when thermal gradients between and amongst surfaces is minimal. The ground-level temperature remains warmer than $T_C$ (negative bias) throughout much of the morning and into the mid-afternoon, when $T_C$ becomes warmer. The bird's-eye and ground-level formulations follow a similar pattern, as expected since both include ground surfaces in their formulation.

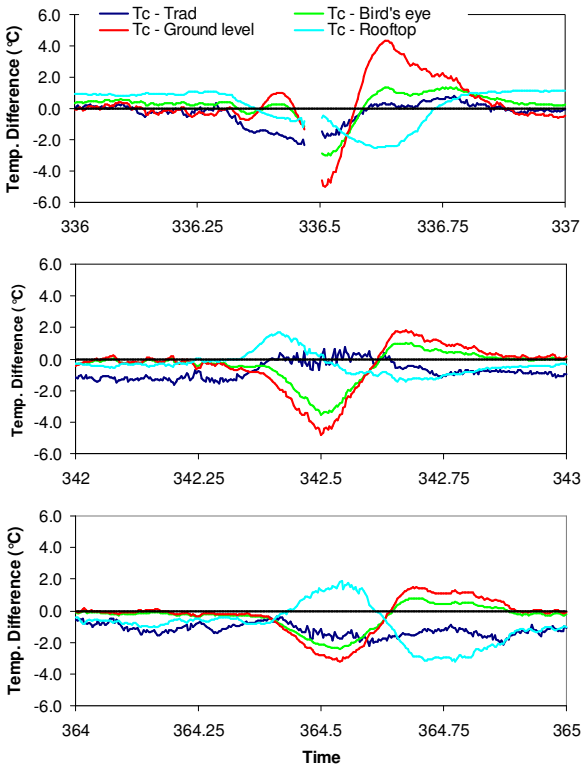


**Figure 4** Comparison of $T_C$ with $T_{rad}$ and the surface temperature from three alternative definitions of the 'complete' urban surface for H/W = 1.25 (top), H/W = 0.63 (middle) and H/W = 0.42 (bottom).

Less overall bias is observed in the bird's-eye formulation, because the temperature pattern of roof surfaces acts to temper the robust thermal response of the ground surface. The best overall diurnal agreement is between $T_{rad}$ and $T_C$, due to the fact that both formulations explicitly include wall surfaces. The view factors of surface components contained within the radiometer FOV, and therefore 'seen' by the CNR1, are given in Table 2. Such differences in agreement between $T_C$ and $T_{rad}$ are attributable to variations in the relative proportion of surface components included in the calculated ($T_C$) and the measured value (upwelling longwave emission, $T_{rad}$) of surface temperature. Agreement between $T_C$ and $T_{rad}$ drops off as canyon aspect ratio decreases. Particularly in the daytime, $T_{rad}$ is warmer than $T_C$ because of the greater proportion of warmer roof and street surfaces contained in the sensor FOV.

**Table 2** Weightings of surface components in a building unit (area-weighted method) and within the FOV of the CNR1 radiometer.

| | % wall | % roof | % street |
|---|---|---|---|
| **H/W = 1.25** | | | |
| Area-weighted | 53 | 21 | 26 |
| CNR1 | 31 | 44 | 25 |
| **H/W = 0.63** | | | |
| Area-weighted | 39 | 15 | 46 |
| CNR1 | 22 | 25 | 53 |
| **H/W = 0.42** | | | |
| Area-weighted | 29 | 11 | 60 |
| CNR1 | 15 | 16 | 69 |

### 4.3 *Modeled effective thermal anisotropy*

The directional variation of upwelling thermal emissions resulting from microscale temperature patterns of the three-dimensional urban surface is termed the effective thermal anisotropy of the surface (Voogt, 2008). Because of this effect, remotely sensed observations of surface temperature tend to be biased as functions of both view direction and time, as compared to the representative surface temperature (defined here as the complete surface temperature $T_C$). In addition to looking at the impact of radiometer height on observed thermal emissions, the SUM model provides the ability to extend the analysis to other viewing angles and azimuths (Voogt, 2008) in order to assess the degree of effective thermal anisotropy arising from off-nadir viewing directions.

Model simulations are performed for the H/W = 0.63 scale model configuration at 0920, 1220, and 1520 local time using a 36° sensor FOV at 5° increments in off-nadir angle and 10° increments in azimuth angle. The sensor height was 19×BH, set to provide maximum coverage of the scale model domain for the largest off-nadir angle and to minimize the dependence of the results on the exact sensor position relative to the scale model surface. Interpolated results are summarized as polar plots (Figure 5).

The plots demonstrate the influence of solar forcing as it affects the microscale surface temperature distribution. The location of a hot spot follows the direction opposite solar azimuth,

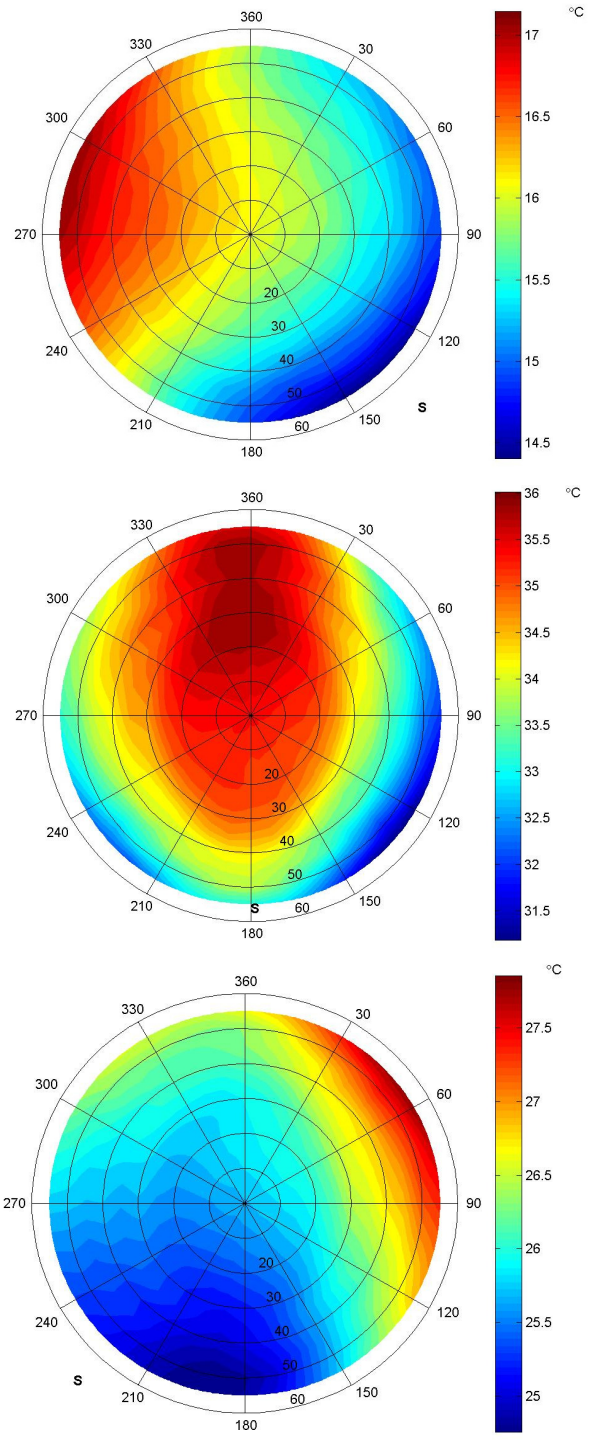


**Figure 5** Modeled directional radiometric surface temperature (℃) over the H/W = 0.63 surface configuration for 0920 local time (top), 1220 local time (middle) and 1520 local time (bottom) for each viewing direction (5° increments in off-nadir angle and 10° increments in azimuth angle) using a 36° FOV sensor at 19BH. **S** indicates the position of the sun.

from northwesterly viewing directions in the morning to northerly view directions near solar noon, and northeasterly view directions in the afternoon. The warmest temperatures are observed at large off-nadir viewing angles towards the north, when the most directly-sunlit south walls and north-south oriented streets dominate the sensor FOV. Temperatures drop off gradually as azimuths increase or decrease from either side of the hot spot region. Large off-nadir viewing angles in the direction of solar azimuth that view the predominantly shaded surfaces (north walls, west walls in the morning, east walls in the afternoon, east-west oriented streets) contain the coolest temperatures.

Anisotropy at solar noon decreases with wider canyon geometry (Figure 6), as expected according to coupled model simulations (Krayenhoff and Voogt, 2007). For all three model configurations nadir view directions are relatively warm, a function of peak roof and street temperatures at this time of day. The overall pattern of anisotropy near solar noon for H/W = 0.42 is very similar to the combined simulations for many points over a light industrial district in Vancouver with the same canyon aspect ratio (Figure 14a Voogt, 2008). The absolute value of anisotropy for the scale model is slightly smaller (2.5℃ compared to 3.5℃) than that from the Vancouver study. The temporal variation of anisotropy shown in Figure 5 is also similar to that shown in the coupled model simulations. These results suggest that the anisotropy generated by the scale model is reasonable, despite the roof configuration of the scaled buildings.

## 5. CONCLUSION

Field observations of urban facet temperatures conducted at an open-air physical scale model are used to further understand the variations in complete urban surface temperature. Three canyon aspect ratios (H/W = 1.25, 0.63, and 0.42) were tested and a surface-sensor-sun numerical model was used to calculate view factors of surfaces 'seen' by a radiometer positioned above the array. The area-averaged complete surface temperature of a building unit ($T_C$) is shown to correspond with longwave emissions ($T_{rad}$) observed at 161 cm above the array (i.e. at approximately 6.4 times the mean building height). Less agreement between $T_C$

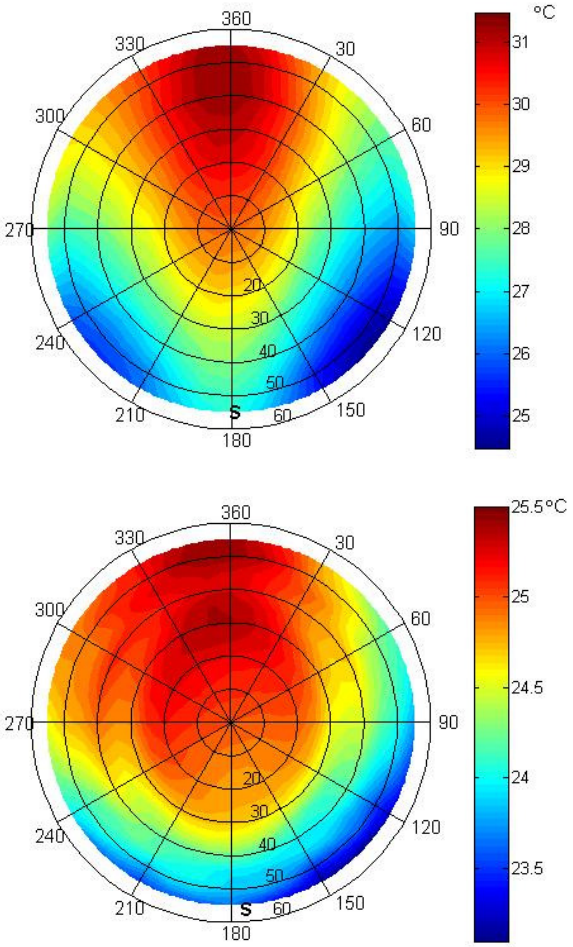


**Figure 6** Modeled directional radiometric surface temperature (°C) over the H/W = 1.25 (top) and H/W = 0.42 (bottom) surface configuration for 1220 local time for each viewing direction (5° increments in off-nadir angle and 10° increments in azimuth angle) using a 36° FOV sensor at 19BH. **S** indicates the position of the sun.

and the surface temperature derived from other common conceptualizations of the urban surface (ground-level, bird's-eye view, and roof-top) was observed, particularly during the day. Facet temperatures were combined with model-generated view factors to assess the degree of effective thermal anisotropy arising from off-nadir viewing directions. The magnitude and pattern of modeled effective thermal anisotropy throughout the daytime and between scale model configurations compare with that from a full-scale light industrial site. The scale model will prove a valuable resource in testing coupled model results of anisotropy for different urban geometries.

## 6. ACKNOWLEDGEMENTS

Thanks are due to R. Martorano, J. Carlson, ASU Research Support Services, and Drs. J. Golden and T. Brazel and for site access and logistical support at ASU. J. Carlson, R. Bhardwaj, T. Otanicar, D. Telford, and Dr. M. Barlage provided helpful assistance in the field and Dr. T. Jones assisted in data processing and management. The FLIR infrared camera was kindly made available by the National Center of Excellence on SMART Innovations at ASU. Funding for this research was provided by the Natural Sciences and Engineering Research Council of Canada.

## 6. REFERENCES

Kanda, M., 2006: Progress in the scale modeling of urban climate: Review. *Theor. Appl. Climatol.*, **84**, 23-33.

Krayenhoff, E.S. and J.A. Voogt, 2007: Combining sub-facet scale urban energy balance and sensor view models to investigate the dependence of effective thermal anisotropy on city structure. 7th Symposium on the Urban Environment, American Meteorological Society, San Diego, California, 4pp.

Mills, G., 1997: Building density and interior building temperatures: a physical modeling experiment. *Physical Geography*, **18**, 195-214.

Oke, T.R., 1981: Canyon geometry and the nocturnal urban heat island: comparison of scale model and field observations. *J. Climatol.*, **1**, 237-254.

Plate, E., 1999: Methods of investigating urban wind field – physical models. *Atmos. Environ.*, **33**, 3981-3989.

Soux, C.A., J.A. Voogt, and T.R. Oke, 2004: A model to calculate what a remote sensor 'sees' of an urban surface. *Bound.-Layer Meteorol.*, **111**, 109-132.

Voogt, J.A., 2008: Assessment of an urban sensor view model for thermal anisotropy. *Remote Sens. of Environ.*, **112**, 482-495.

Voogt, J.A. and T.R. Oke, 1997: Complete urban surface temperatures. *J. Appl. Meteorol.*, **36**, 1117-1132.